

Amplification measurements of alternative imaging gases in environmental SEM

A L Fletcher, B L Thiel and A M Donald

Polymer and Colloids Group, Cavendish Laboratory, University of Cambridge, Madingley Road, Cambridge, CB3 0HE, UK

Received 26 November 1996, in final form 21 March 1997

Abstract. In this paper, we present quantitative data on the amplification behaviour of alternative imaging gases in environmental SEM and describe the experimental methods used to obtain them. We investigated the gases' amplification abilities over the pressure range 0–12 Torr with respect to the primary beam energy, detector gap distance and detector accelerating field, in order to isolate optimum imaging conditions for each gas. The gases investigated were, in addition to water vapour, nitrous oxide, carbon dioxide, nitrogen and helium.

1. Introduction

The environmental scanning electron microscope (ESEM) detection system is unique in the fact that it relies on the presence of a gas in the chamber; it is the choice of this gas that is critical for determining the image quality. Many commercial instruments use a secondary electron detection system that depends upon secondary electrons' interactions with gaseous molecules to produce a 'cascade' effect amplification. This cascade effect is illustrated in figure 1. The detector is a positively biased annular electrode placed directly above the sample, which creates a field between the two. The beam enters through a hole in the detector and hits the sample. Low-energy secondary electrons are emitted from the sample and are accelerated by the field through the gas towards the detector. Once an electron has attained the ionization energy of the gas, it is able to undergo ionizing collisions which produce a further electron (termed an 'environmental' secondary electron) and a positive gaseous ion. The environmental electron is then accelerated towards the detector. Along its path, the environmental electron goes on to have its own ionizing collisions. In this way a cascade effect takes place, resulting in many electrons—derived from the original—reaching the detector. These are then processed to form an image. By proper selection of the gas type, gas pressure, working distance and detector accelerating field, it will be shown in this paper that an original secondary electron can be amplified over 1000 times.

In the same way that the electrons are accelerated towards the detector, the positive ions are swept towards the sample. They neutralize the build up of negative charge on the sample and therefore remove the need for a conductive coating to be applied to most insulating samples. However, if the net flux of electrons to the sample is significantly less

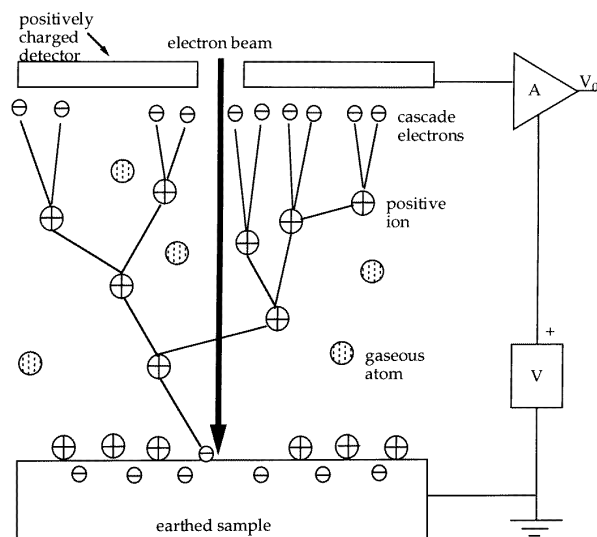


Figure 1. A schematic diagram of the amplification process due to the collisions between the secondary electrons and gaseous molecules.

than that of the positive ions, then positive charging will occur. It is therefore important to obtain the correct balance to achieve a good quality image.

This type of gas cascade amplification system also amplifies background and spurious noise signals, since electrons from any source will be amplified and collected. Therefore, the signal collected by the detector is necessarily not a 'pure' secondary electron signal from the sample, but rather a composite of several sources. The relative contribution of background sources is one factor in determining the final quality of the image, which is discussed in the background theory and discussion sections.

Readers are directed to the paper by Thiel *et al* [1] for a more thorough discussion of the origin of the image signal.

The gain of the gas cascade system is inherently limited because the gas has a finite amplification capacity, beyond which electrical breakdown occurs. Breakdown occurs under two conditions. First, if the bias on the detector is high at small working distances, then dielectric breakdown of the gas occurs and arcing is seen. Second, at long working distances the saturation current of the gas can be attained, at which point the gas becomes a conductive medium and amplification is no longer possible [2].

Although it is a crucial mechanism for image contrast, quality and interpretation, the amplification is only now being understood and has not been characterized well. It is highly dependent on many of the operating parameters of the ESEM, in particular the imaging gas type. Conventionally, water vapour is the gas used. Not only does it exhibit one of the highest ionization efficiencies of any pure gas but also it is useful for many *in situ* experiments involving hydration, dehydration and wet-sample imaging. However, for many experiments it is crucial that no water vapour be present, for example when observing or avoiding certain chemical reactions or when carrying out experiments below 0°C. To investigate the suitability of gases for cryogenic imaging, we designed a system to measure quantitatively the amplification properties of gases as a function of ESEM operating parameters. These investigations complement our theoretical models for the gas amplification process [1].

2. The background theory

The cascade process described here can be thought of, to a first approximation, as a Townsend gas capacitor (TGC). A comprehensive text concerning the TGC physics and the ionization of gases in an electric field was the work of von Engel in 1965 [3]. Several authors have since advanced this model to apply it directly to high-pressure SEM and ESEM [4–8]. On the basis of our early amplification measurements, obtained using the methodology described in this paper, it became clear that, although they are qualitatively correct, these models do not predict quantitatively the cascade process as it occurs in the ESEM, in particular its pressure dependence. Our group has advanced a modified theory that describes more accurately the cascade process as it happens in the ESEM [1]. This theory, briefly outlined below, will be used to interpret our experimental data on the amplification behaviours of various gases.

The amplified ESEM signal derives from four sources: secondary electrons (SE), backscattered electrons (BSE), primary electrons scattered from the primary electron beam (PE) and electrons emitted from the sample surface due to positive-ion impact. Each source is amplified by the cascade but in different ways due to differences in their energies. It is the SE that provide the important topographic information and the BSE are responsible for some atomic-number contrast, whereas the PE and positive-ion-impact electrons add to the background signal.

Consider first the amplification of the secondary electrons [3]. A low-energy SE produced at the sample surface is accelerated by the field, which is created by the positive voltage V applied to the detector. It traverses the distance between the sample and the detector, a distance d_{gap} . Let this electron produce at any point α electrons and α positive ions per unit length along its path, by means of ionizing collisions with the gaseous molecules. The coefficient α , known as Townsend's first ionization coefficient, depends on the field, gas pressure and gas type. We have realized that understanding how α changes as a function of the position in the gap is the crux of all amplification considerations [1].

If α is treated in the first instance as being constant throughout the gap, as in the original TGC theory, then the increase in the number of ion pairs produced along an element dx of the gap is αdx per secondary electron. By integrating between 0 and d_{gap} , we find the number of electrons reaching the detector, N_d , as a function of the number of electrons produced at the sample surface, N_0^- , to be

$$N_d = N_0^- \exp(\alpha d_{gap}). \quad (1)$$

From this equation, it is obvious that the current increases exponentially with increasing gap distance. This equation makes a number of simplifying assumptions that are not strictly appropriate under most ESEM operating conditions. These concerns have been treated in the paper by Thiel *et al* [1], in which we proposed a model which shows that α cannot be treated as constant throughout the gap. In that paper we replaced d_{gap} by an effective gap distance, D_{eff} . Furthermore, α was replaced by a limiting value α_∞ . Equations for determining D_{eff} and α_∞ were provided in [1]. Remembering that the number of positive ions is one less than the electron current because of the original SE, equation (1) can be modified to show that the positive ion current I^+ produced by a primary beam current I_0 impinging upon a surface of secondary electron emission coefficient δ is given by

$$I^+ = I_0 \delta [\exp(\alpha_\infty D_{eff}) - 1]. \quad (2)$$

The rate at which environmental electrons are produced by PE and BSE is lower than the rate of production by low-energy SE, due to their higher energy and consequently lower ionization cross section. The current due to environmental electrons produced by PE is dependent on the primary beam current, I_0 , the ionization efficiency of PE (S_{pe} in ion pairs $\text{mm}^{-1} \text{Torr}^{-1}$), the gas pressure P and the distance travelled by the electrons, d_{gap} . The BSE-derived signal is dependent similarly on I_0 , P , d_{gap} , the ionization efficiency of BSE (S_{bse} in ion pairs $\text{mm}^{-1} \text{Torr}^{-1}$) and also on η , the backscattered electron emission coefficient of the sample.

Finally, environmental electrons are produced from the fourth source, positive ion impact at the sample surface. When this occurs, further electrons are liberated with an efficiency γ . A positive ion that hits the specimen surface is therefore amplified successively by equation (2) to give a gain factor of k , which is defined to be

$$k = 1 + \gamma [\exp(\alpha_\infty D_{eff}) - 1] + \gamma^2 [\exp(\alpha_\infty D_{eff}) - 1]^2 + \dots \quad (3)$$

So the total signal reaching the detector is derived from these four sources, namely secondary, backscattered, primary and positive ion impact electrons. When all four sources of signal are considered, the total positive ion current I^+ is found to be given by [1]

$$\frac{I^+}{I_0} = k[\exp(\alpha_\infty D_{eff}) - 1] \left(S_{pe} \frac{P}{\alpha_\infty} + \delta + \eta S_{bse} \frac{P}{\alpha_\infty} \right). \quad (4)$$

Equation (4) can be used to anticipate the relative contributions of the four sources under various operating conditions and the trends predicted by this equation were used to interpret our experimental amplification profiles. For example, figure 2(a) shows the shape of the amplification profile of each source predicted by equation (4). This was over the pressure range 0–15 Torr, for an amorphous carbon surface in water vapour at a gap distance of 6.5 mm. In water vapour, von Engel [3] estimated γ to be around 10^{-10} , making the effect of positive ion impact negligible. It can be seen that each contribution peaks at a pressure in the range 2–3 Torr and that the main contribution at the peak pressure is from the SE. It is worthy of note that the PE contribution starts to rise slightly at the high-pressure end. Figure 2(b) shows the predicted percentage contributions of the SE-derived signal, the BSE-derived signal and the PE-derived signal. It can be seen that the BSE contribution to the overall signal is always relatively small. The SE contribution dominates at low pressure, but, under the working conditions chosen, the PE background signal dominates above around 6 Torr.

3. The experimental apparatus

The amplification is defined in this paper as the ratio of the total ion current to the number of electrons that leaves the sample surface, as is explained in the next section. In order to evaluate the amplification, two sets of measurements were taken: the primary electron-beam current and the positive ion current. The positive ion current was measured rather than the cascaded electron signal at the detector because the detector signal was difficult to isolate. It also contained noisy electron signals scattered from the pole piece and other internal chamber surfaces. Once the two measurements had been performed, the ion current was normalized with respect to the primary electron-beam current and the secondary electron and the backscattered electron coefficients, δ and η , of carbon. This calculation is described in the next section.

We designed a Faraday cage that, with small modifications, was able to measure both the primary electron-beam current and the positive ion current. The set-up in figure 3 shows how the primary electron-beam current was measured. The Faraday cup was made of amorphous carbon, which has well-tabulated secondary emission coefficients. First, the beam was focused through a 300 μm plastic aperture, which had been coated with electrically conducting silver dag, and then through a 30 μm platinum aperture on to the bottom of the cage. The cage was 1.4 mm deep. The top of the plastic aperture was electrically connected to a ‘guard’ ring that had a bias

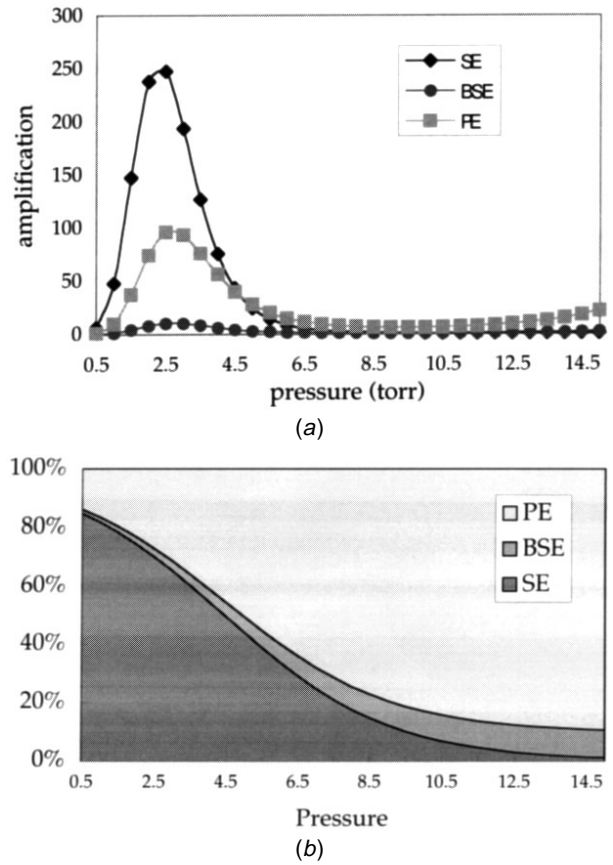


Figure 2. (a) A graph showing the shape of the variation in amplification with pressure for the secondary electrons (SE), the backscattered electrons (BSE) and the primary electrons (PE). This was calculated for 20 keV primary beam electrons hitting an amorphous carbon surface, from equation (4) for water vapour at a detector gap distance of 6.5 mm and a detector bias of 433 V. (b) A graph showing the percentage contributions to the signal from the SE, BSE and PE. This was calculated from equation (4) for water vapour at a detector gap distance of 6.5 mm and a detector bias of 433 V.

of -36 V applied to ensure that any positive ions created in the chamber by the beam being scattered on its way down were collected and did not reduce the primary electron-beam current being read. The detector bias was also kept at its minimum of $+30$ V so that the cascade process was minimized. The backscattered electrons were trapped in the cage and collected by the platinum aperture, which was in electrical contact with the cage. Any secondary electrons ejected from the carbon cup were not accelerated and eventually were re-collected by the cage. The primary electron-beam current was taken from the centre of the cage, as shown, and was read by a sensitive electrometer.

Then the Faraday cage was modified to read the positive ion current resulting from the cascade. Since each ionizing collision gives one electron and one positive ion then, apart from the original secondary electron, the positive ion current is a measure of the cascade amplification. For this measurement, the two apertures and the guard ring were removed and the beam was focused onto the bottom of the cage. The detector bias was set to between $+250$ and $+520$ V, which created a field sufficient to accelerate

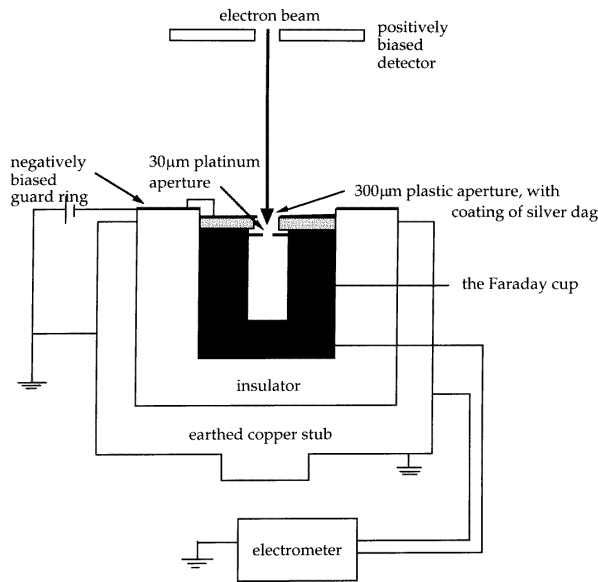


Figure 3. The Faraday cage set-up used to measure the primary electron-beam current. It is modified slightly by removing the two apertures to measure the ion current.

the secondary electrons towards the detector and initiate a cascade. The positive ions were swept towards the cage by the field and read by the electrometer. The positive current reading was partially neutralized by the probe-beam current, but this was compensated for in the calculation of amplification.

4. The calculation of the amplification

Under the assumption that the negative guard ring kept any stray positive ions in the chamber away from the cage, the negative current read did indeed correspond to the primary electron-beam current reaching the sample surface (backscattered electrons were trapped in the cage and collected and the secondary electrons just recombined in the carbon). To calculate the total amplification, the number of electrons leaving the sample that went on to cause the cascade had to be determined. This is the primary electron-beam current (I_{pe}) multiplied by each of the backscattered-electron coefficient (η) and the secondary electron coefficient (δ) of carbon and summed. Both η and δ vary with the gun voltage, as shown in figure 4. This was obtained from the program SE_MC written by Joy [9]:

$$\text{Number of SE leaving the sample per second} = I_{pe}(\eta + \delta). \quad (5)$$

The positive ion current that is read by the electrometer, I_{meas} , is negated by all the primary electron-beam electrons, with the exception of the ones that are backscattered. So the true ion current, I^+ , is given by the following expression:

$$I^+ = I_{meas} + I_{pe} - \eta I_{pe}. \quad (6)$$

So, that to which we will refer as the amplification is the ratio of the ion current to the number of electrons

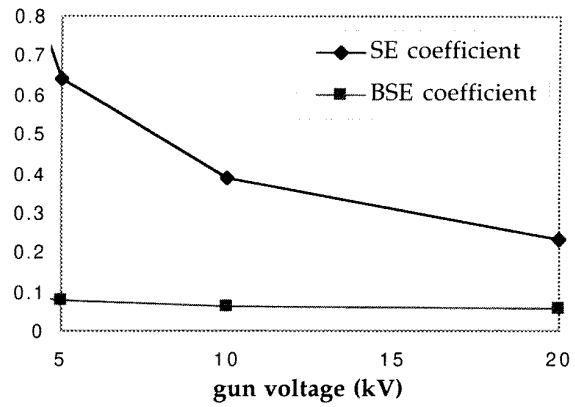


Figure 4. The dependences of the backscattered and secondary electron emission coefficients (η and δ) of amorphous carbon on the primary beam energy [9].

leaving the sample, which is

$$\text{amplification} = \frac{I_{meas} + I_{pe} - \eta I_{pe}}{I_{pe}(\eta + \delta)}. \quad (7)$$

5. The experimental method

Three sets of experiments were performed to isolate the effects of varying the primary beam energy, the detector gap distance and the detector accelerating field, with each of the gases. In addition to water vapour, the gases investigated were carbon dioxide, nitrous oxide, nitrogen and helium. In each experiment the pressure range was swept from 0 to 12 Torr in steps of 1 Torr.

(i) The variation of ion current was measured for primary beam energies of 10, 15, 20 and 25 keV. The detector gap distance was chosen to be relatively large at 6.5 mm (since a 5 mm bullet was used, the detector gap distance was the working distance less 5 mm) to give a large peak amplification. The detector bias was set to 350 V. This was chosen to be low in order to avoid sample charging. To normalize these readings, the primary electron-beam current was measured under similar conditions, but with the detector set at its minimum value of 30 V.

(ii) The variation in ion current was measured as a function of the detector-to-sample gap distance. Detector gap distances of 4.5, 5.5, 6.5 and 7.5 mm were used. The detector bias was set to 300, 366, 433 and 500 V respectively, which corresponded to a constant accelerating field of 66.7 V mm⁻¹. The primary beam energy used was 20 keV. The primary electron-beam current was once again taken over the pressure range under similar conditions, with the detector bias set at 30 V.

(iii) The third experiment investigated the effect of the detector accelerating field on the amplification profile. Again a detector gap distance of 6.5 mm was used and the detector bias was stepped up to 300, 400 and 500 V, corresponding to accelerating fields of 46, 62 and 77 V mm⁻¹. This was done at a primary beam energy of 20 keV.

The positive ion current readings were normalized with respect to the primary electron-beam current taken with a detector bias of 30 V, rather than 300, 400 and 500 V. It was assumed that having a large detector bias did not physically affect the incident electron beam, but did affect the measured current on the electrometer. This was because many more positive ions were created in the chamber, increasing the likelihood of their leaking into the cage and partially negating the reading of the probe beam.

6. Results

Once the readings of the primary electron-beam and positive ion currents has been taken, the amplification was calculated as a function of the pressure according to equation (7). The results show quantitatively how each gas behaved with respect to the primary beam energy, working distance and detector accelerating field. The trends shown in the data were reproducible, but the absolute values of the primary electron-beam and ion currents were difficult to repeat from day to day. The features that are worthy of note are the position, amplitude and breadth of the peak amplification and the level of the high-pressure plateau.

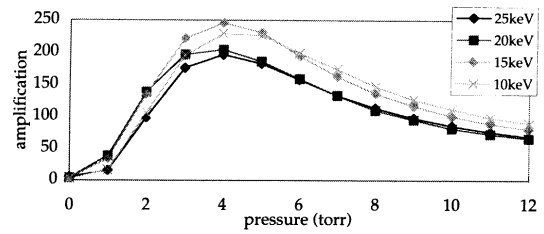
6.1. The dependence of the amplification on the primary beam energy

The amplification curves for all the gases with respect to the primary beam energy are shown in figures 5(a)–(e). From figures 5(a)–(e) it is apparent that the position and breadth of the peak do not depend on the primary beam energy with any of the gases; however, the amplitudes of the peak and the plateau do. In water vapour the peak amplification occurred at 4 Torr and the amplification values were similar for all energies. In comparison, for carbon dioxide the amplification peaked in the range 2–3 Torr and was significantly smaller at 25 keV than it was for other primary beam energies. Also, in water vapour the high-pressure plateau levels were similar in all cases, whereas in carbon dioxide the levels appeared to be dependent on the primary beam energy.

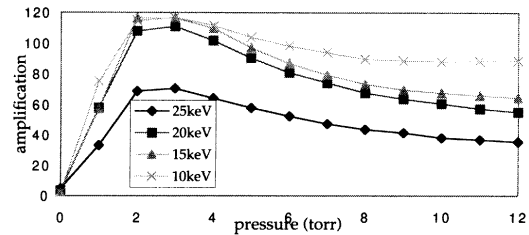
The breadths of the amplification peaks for nitrous oxide and nitrogen were narrow compared with those for water vapour and carbon dioxide. In both cases the peak amplification occurred at 2 Torr. In contrast to the other gases, the electron amplification in nitrogen peaked highest at 25 keV. It is also noteworthy that the plateau amplification value was lowest at 25 keV; the relevance of this will be discussed in section 7.

6.2. The dependence of the amplification on the detector gap distance

Figures 6(a)–(e) show the way in which the amplification varied for each gas with respect to the detector gap distance. It can be seen that the amplitudes of the peak and the plateau are dependent on the gap distance. Also water vapour, in common with carbon dioxide and nitrous oxide, showed a tendency for the peak amplification to shift to slightly higher pressures at longer detector gap distances.



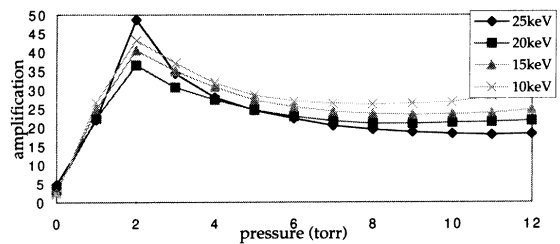
(a) water vapour



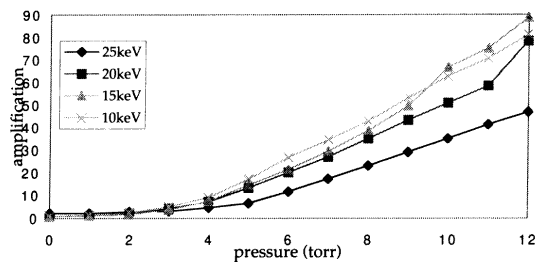
(b) carbon dioxide



(c) nitrous oxide



(d) nitrogen



(e) helium

Figure 5. The dependences of the amplification on the pressure for various primary-beam energies in the five gases (detector gap distance 6.5 mm, detector bias 350 V): (a) water vapour, (b) carbon dioxide, (c) nitrous oxide, (d) nitrogen and (e) helium.

At 7.5 mm in carbon dioxide, nitrous oxide and nitrogen, a small degree of arcing occurred which may account for the uneven profiles of the curves. Again, nitrous oxide and nitrogen exhibited a sharper peak amplification profile and,

on comparing figures 6(a)–(e), it can be seen that nitrogen gave a significantly smaller amplification than did the other gases.

6.3. The dependence of the amplification on the detector accelerating field

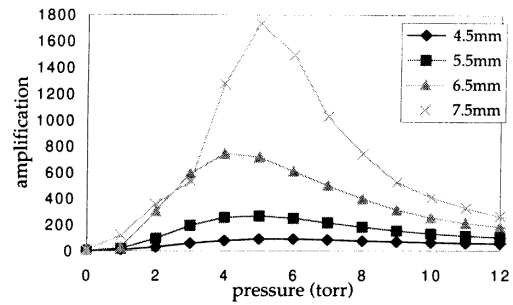
From figures 7(a)–(e), which show the dependence of the amplification on the detector bias and hence on the accelerating field, it can be seen that the amplitudes of the peak and plateau values vary with different accelerating fields. With each gas, the amplification profile was shallow and the peak small at low detector accelerating field. As the field was increased, an approximately exponential increase in amplification was observed. In water vapour, the system arced too much at 500 V detector bias for us to take sensible readings so a peak could not be observed. In nitrogen a smaller bias of 450 V was used for the same reason.

6.4. Helium data

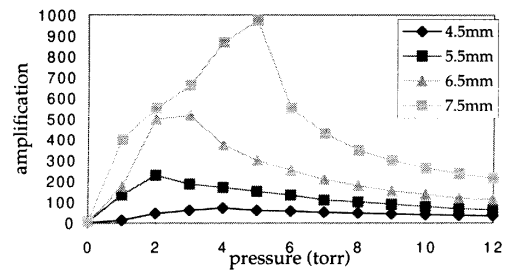
Helium was shown to be anomalous in all situations, as can be seen in figures 5(e), 6(e) and 7(e). Figure 5(e) shows that, over the pressure range investigated, the amplification did not peak but rather kept on increasing. Although not shown on the plot, the amplification increased until the pressure reached 18 Torr, at which point the rotary pump could not maintain the vacuum in the chamber—helium was a difficult gas to pump on account of its small atomic size. The working distance data, shown in figure 6(e), show that the amplification appeared to peak. However, this is thought to have been due to the system arcing at 5.5 and 6.5 mm detector gap distances and the measurements taken were the average electrometer reading during arcing. For this reason, it is believed that the true curves would look more like the 4.5 mm curve. Similarly, in figure 6(e), at a detector accelerating bias of 350 V the system arced so no more readings were taken.

7. Discussion

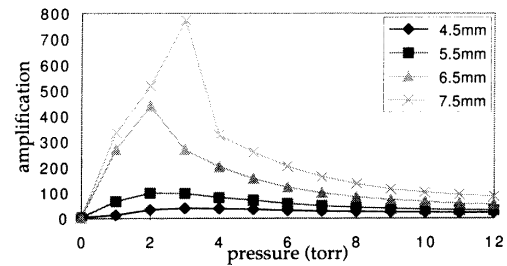
It was shown in the results section that the amplification behaviour of each gas was distinctive. The shape of the profiles, in all cases besides helium, followed the general shape predicted by figure 2(a), which was obtained from equation (4) in the theory section. In terms of peak amplification it can be seen that, under similar conditions, water vapour gives quantitatively the largest maximum amplification, followed in order by carbon dioxide, nitrous oxide and nitrogen. At first sight it may appear that the magnitude of this peak amplification will determine the quality of images that can be achieved with a particular gas. However, the amplification curves shown in figures 5–7 demonstrate that the shape of the peak, the pressure at which the peak occurs and the amplification in the high-pressure tail region also all vary from gas to gas. Outlined below are the factors that determine the shape of the amplification profiles and play a role in determining the suitability of each gas for imaging.



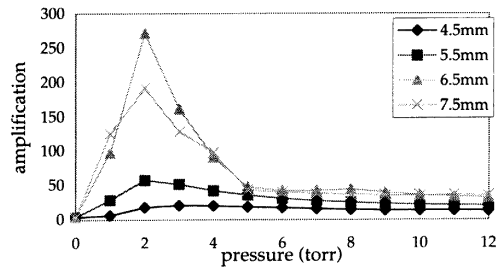
(a) water vapour



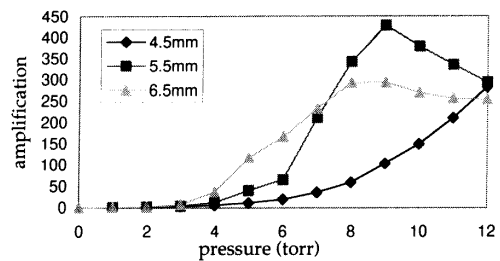
(b) carbon dioxide



(c) nitrous oxide



(d) nitrogen



(e) helium

Figure 6. The dependences of the amplification on the pressure for various detector gap distances in the five gases (primary beam energy 20 keV, constant accelerating field of 66.7 V mm⁻¹): (a) water vapour, (b) carbon dioxide, (c) nitrous oxide, (d) nitrogen and (e) helium.

Table 1. Peak-to-plateau ratios of the gases under various conditions of primary beam energy and detector gap distance.

Primary beam energy (kV)	Water vapour			Carbon dioxide			Nitrous oxide			Nitrogen		
	Peak amp.	Plat. amp.	Ratio	Peak amp.	Plat. amp.	Ratio	Peak amp.	Plat. amp.	Ratio	Peak amp.	Plat. amp.	ratio
10	229	90	2.5	116	88	1.3	58	29	2.0	43	29	1.5
15	246	80	3.1	117	65	1.8	66	27	2.4	40	25	1.6
20	204	66	3.1	111	56	2.0	71	29	2.5	37	22	1.7
25	196	69	2.8	70	35	2.0	51	23	2.2	49	18	2.7
Gap (mm)												
4.5	88	42	2.1	70	34	2.1	39	20	2.0	21	13	1.6
5.5	264	67	3.9	186	62	3.0	97	29	3.3	58	20	2.9
6.5	742	113	6.6	519	110	4.7	440	53	8.3	271	32	8.5
7.5	1732	109	15.9	974	214	4.6	771	83	9.3	191	35	5.5

7.1. The peak-to-plateau ratio

As was discussed in the theory section, the amplification is a combination of four signals, those derived from SE, PE and BSE plus SE from positive ion impact. The graph obtained from equation (4), seen in figure 2(b), shows that, with water vapour, the SE-derived signal dominates at low pressure, but is gradually overtaken by the background PE signal as the pressure is increased. The BSE signal always remains relatively small and, for water vapour, the contribution due to positive ion impact is negligible. There are three further factors that may affect the amplification behaviour and which have not been considered in the theory section. These are recombination of the charge carriers in the gas, which would reduce the amplification; space-charge effects, whereby positive ions may collect above the sample and recombine with the SE emanating from the surface; and electronegativity of the gas, by which signal electrons can collide with the gaseous molecules to form negative ions. Reference [1] explains why we believe these effects are negligible in water vapour. However, how they affect the signal in the other gases is not known and will not be speculated upon here.

From figure 2(b), we conclude that the tail, or plateau, region at the high-pressure end of the amplification profiles (observed in all cases except helium) is predominantly made up of signal created by the PE scattering out of the beam. Since the PE contain no image information they contribute to the background signal, which is why, at higher pressures, contrast is reduced. It can also be inferred from figure 2 that the lower the pressure the more likely it is that the image is due to the SE, which carry the topographical image information. So at the peak amplification, which occurs at intermediate pressures, the signal is derived from both. It can therefore be concluded that the extent to which the image information is obscured by the background (that is, the useful signal-to-noise ratio) is shown by the peak-to-plateau ratio of the amplification curves. Hence, the peak-to-plateau ratio can serve as a useful quantitative indication of the image potential of a gas—the higher the ratio the less the relative contribution from the background signal and the more suitable the gas for imaging under the particular instrument conditions.

7.2. The primary beam energy

Table 1 shows the peak amplification, the plateau amplification and the ratio of the two under all the conditions of primary beam energy and detector gap distance investigated. From the primary beam-energy results it can be seen that water vapour consistently gave the highest peak-to-plateau ratio, followed in order by nitrous oxide, carbon dioxide and nitrogen. Experience has shown that this is the order in which the imaging qualities of the gases rank. For each gas, the lowest ratio was at 10 keV, indicating that images at this primary beam energy will have a greater background contribution which will obscure the sample information. This is consistent with the fact that the ionization cross section for high-energy electrons, namely the PE and BSE, is higher at lower primary beam energies. For water vapour and nitrous oxide, the highest ratios were achieved at 20 and 15 keV, whereas with carbon dioxide and nitrogen the highest ratios were at 20 and 25 keV, so it can be concluded that the best images will be obtained at different primary beam energies, depending on the gas being used.

7.3. The detector gap distance

The detector gap distance curves (figures 6(a)–(e)) in the results section show that the dependence of the amplification on the detector gap distance was similar for each gas. A small, shallow profile was obtained at 4.5 mm and, as the detector gap distance was raised in a stepwise manner to 7.5 mm, the peak amplification increased substantially. This was expected from the theory of amplification, particularly equation (1) in the theory section, which shows that the amplification is exponentially dependent on d , the detector gap distance.

From the peak-to-plateau ratios in table 1 for the working distance results, it can be seen that the general trend is for the ratio to increase as the working distance increases. However, a trade-off is made; with long working distances, in all gases, there is a tendency for the amplification to become so large that arcing occurs and the image is obliterated. Also, the longer the working distance the more the beam is broadened by the probe electrons

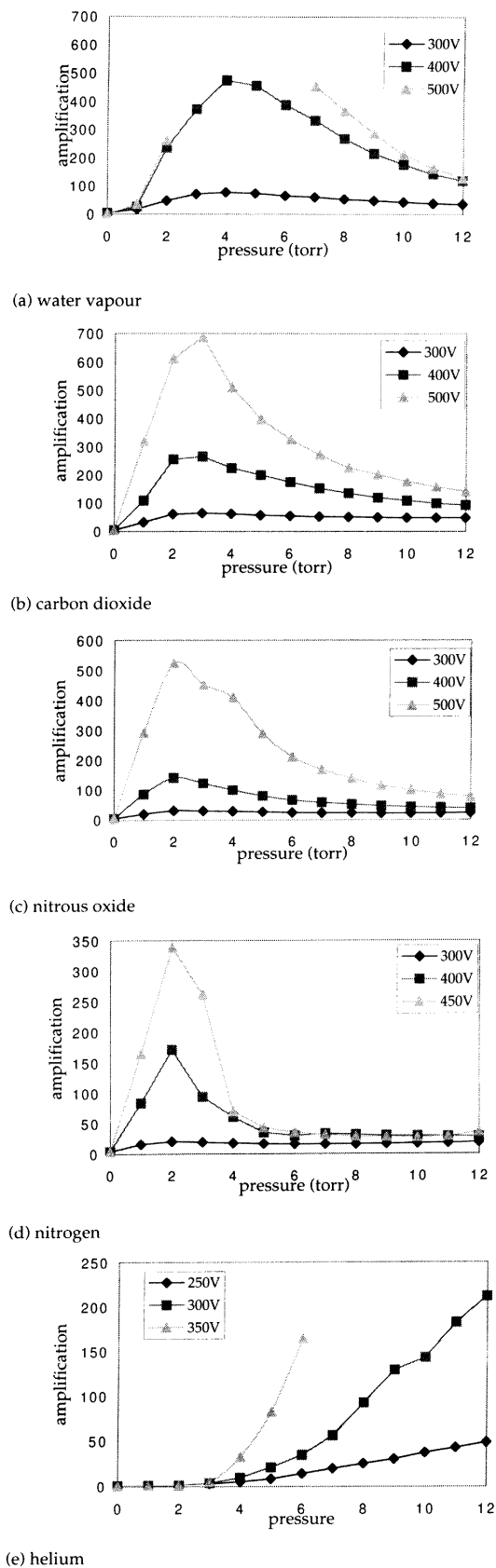


Figure 7. The dependences of the amplification on the pressure for various detector biases in the five gases (primary beam energy 20 keV, detector gap distance 6.5 mm): (a) water vapour, (b) carbon dioxide, (c) nitrous oxide, (d) nitrogen and (e) helium.

undergoing non-ionizing collisions with gaseous molecules, whereby spatial resolution is lost.

Both in carbon dioxide and in nitrous oxide, the peak amplification occurred at higher pressure as the detector gap distance was increased. This shift in peak was unexpected and has not been explained by the theory as it currently stands. For carbon dioxide, the peak shift meant that the maximum amplification occurred at 3 Torr at 6.5 mm and at 5 Torr at 7.5 mm. This could have been due to the effect of charging, which was observed with carbon dioxide but not with the other gases under these conditions.

7.4. The behaviour with helium

The amplification of helium was anomalous compared with the data from the other gases; no peak was observed over the pressure range investigated. It was the only monatomic gas to be investigated and its inelastic and ionization collision cross sections are less complex than those of larger, molecular gases since internal vibrational modes are absent. It is therefore unsurprising that the amplification of helium behaved in a different manner. Experience has shown that its imaging behaviour is also different from those of the other gases—an image can be maintained at relatively high pressures of up to around 13 Torr. Inspection of equation (4) may help explain this. On the basis of ionization cross sections, S_{pe} and S_{bse} for helium are approximately an order of magnitude smaller than those for water vapour [10, 11]. Consequently the SE contribution to the signal dominates over the entire pressure range investigated.

8. Conclusions

The cascade process occurring in ESEM, by which image information is formed and collected, had previously not been investigated in detail. Our novel Faraday cage design has been able to isolate both the primary electron-beam current reaching the sample and the positive-ion current created by the cascade successfully. In this way, we have been able to determine the amplification occurring under systematically varied ESEM operating conditions, for the purpose of investigating the amplification behaviours of various imaging gases in a quantitative manner. Our results have led to two important conclusions. First, the experimentally observed discrepancy between amplification measurements in water vapour and the predictions of the TGC theory has led to a more refined approach to the ionization physics involved. The water vapour data can now be modelled [1] and our understanding of gas ionization physics as it occurs in the ESEM has been improved greatly. Second, optimum operating conditions for each of the gases investigated have been identified in a quantitative way and it has been concluded that the peak-to-plateau ratio of the amplification profiles is likely to give a useful indication of the quality of images which can be achieved in a particular gas. Combining these conclusions has led to an increased awareness of how images are affected by the cascade process, the type of gas and the relative contributions to the signal of various imaging electron species.

Acknowledgments

The authors wish to acknowledge Mr Andrew Eddy for technical support and Dr Paul Meredith for initiating the investigations. This work was funded by the BBSRC, Unilever and the Colloid Technology Programme (jointly funded by the DTI, Unilever, Schlumberger, ICI and Zeneca).

References

- [1] Thiel B L, Bache I, Fletcher A L, Meredith P and Donald A M 1997 *J. Microsc.* **187** pt 3
- [2] Meek J M and Craggs J D 1978 *Electrical Breakdown of Gases* (New York: Wiley)

- [3] von Engel 1965 *Ionised Gases* (Oxford: Clarendon)
- [4] Moncrieff D A, Robinson V N E and Harris L B 1978 *J. Phys. D: Appl. Phys.* **11** 2315–25
- [5] Durkin R and Shah J S 1993 *J. Microsc.* **169** 33–51
- [6] Shah J S and Durkin R 1992 Experimental measurements of amplification in high pressure SEM 1-109-110 *Proc. 10th Eur. Congr. on Electron Microscopy (Granada, 1992)* ed A Ríos *et al* (Granada: Secretariado de Publicaciones de la Universidad de Granada) pp 109–10
- [7] Farley A N and Shah J S 1990 *J. Microsc.* **158** 389–401
- [8] Farley A N and Shah J S 1990 *J. Microsc.* **158** 379–88
- [9] Joy D C 1987 *J. Microsc.* **147** 51–64
- [10] Dayashankar and Green A E S 1992 *Radiat. Phys. Chem.* **40** 523–8
- [11] Alkhazou G D 1970 *Sov. Phys.–Techn. Phys.* **15** 66–73